Accepted Manuscript

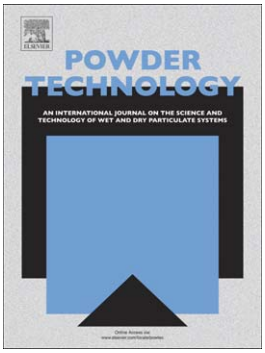

Enhanced photocatalytic properties of reusable TiO_2-loaded natural porous minerals in dye wastewater purification

Bin Wang, Fernanda Condi de Godoi, Shuilin Zheng, Ian R. Gentle, Congju Li

PII: S0032-5910(16)30569-1
DOI: doi: 10.1016/j.powtec.2016.09.003
Reference: PTEC 11913

To appear in: *Powder Technology*

Received date: 31 May 2016
Revised date: 20 August 2016
Accepted date: 1 September 2016

Please cite this article as: Bin Wang, Fernanda Condi de Godoi, Shuilin Zheng, Ian R. Gentle, Congju Li, Enhanced photocatalytic properties of reusable TiO_2-loaded natural porous minerals in dye wastewater purification, *Powder Technology* (2016), doi: 10.1016/j.powtec.2016.09.003

Enhanced photocatalytic properties of reusable TiO_2-loaded natural porous minerals in dye wastewater purification

Bin Wang [a,b] , Fernanda Condi de Godoi [c], Shuilin Zheng [d,*], Ian R Gentle [e] and Congju Li [b,*]

[a] *School of Material Science and Engineering, Beijing Institute of Fashion Technology, Beijing 100029, PR China;*
[b] *Beijing Institute of Nanoenergy and Nanosystems, Chinese Academy of Sciences, Beijing 100083, PR China;*
[c] *School of Agriculture and Food Sciences, The University of Queensland, Brisbane Qld 4072, Australia;*
[d] *School of Chemical and Environmental Engineering, China University of Mining & Technology, Beijing 100083, PR China;*
[e] *School of Chemistry and Molecular Biosciences, The University of Queensland, Brisbane Qld 4072, Australia;*

**Corresponding author: Fax: +86-10-82854885; Email: congjuli2016@163.com,*

Abstract

Diatomite-based recyclable photocatalysts containing single lanthanide doped TiO_2 nanoparticles (NPs) were synthesized by using simple sol-gel method. Photocatalytic activities of the prepared Ce- or La- single doped TiO_2/diatomite catalysts were estimated by the degradation of Rhodamine B (RhB) under simulated sunlight irradiation. The XRD and Raman spectra shown only anatase phase of TiO_2 for the un-doped and Ce-doped samples. The TEM images revealed uniform distribution of TiO_2 NPs on the matrix, indicating that diatomite played an important role to prevent the agglomeration of TiO_2 NPs. Ce-TiO_2/diatomite showed a red shift in UV-visible light absorption edge with enhanced absorption intensity than un-doped sample, whereas La-TiO_2/diatomite showed a blue shift. The bandgap energy of 1.5%-Ce doped sample is as low as 2.75 eV. The XPS spectra showed the presence of both Ce^{3+} and Ce^{4+} oxidation states for Ce dopant. The photoluminescence spectra of the Ce-doped samples showed first decrease in the recombination centers with the maximum decrease for 1.5%-Ce doped sample and then started increase with the increasing Ce in the samples. As compared to the La-doped samples, a desired behavior was observed for the Ce-doped hybrid due to the redox Ce^{4+}/Ce^{3+} pairs acting as electron scavengers and localized unoccupied Ce 4*f* level narrowing the band gap. The incorporation with diatomite as support of TiO_2 nanoparticles is contributed for the improved reusability and also gives a promising strategy to enable the application of nano-photocatalysts in a real wastewater remediation treatment.

Key words: Diatomite; Doping TiO_2; Sol− gel method; Photocatalytic degradation

1 Introduction

All across the world, the impacts caused by environmental pollution on public health represents a remarkable concern. The World Health Organization (WHO) estimates that the prolonged exposure to environmental pollution is responsible by around a quarter of the diseases faced by the population today. Therefore, finding alternatives to remediate and reduce the current environmental pollution is crucial. Photocatalysis technology has the potential to provide solutions to environmental pollution and, consequent, destruction. The key strategy of photocatalysis consists of developing photocatalysts with the ability to harness the solar energy for sustainable and cost-effective processes.

Titanium dioxide (TiO_2) is well-known by its potential use as photocatalyst in degradation systems of hazardous pollutants in water, air and on the solid surfaces, which can cause adverse effects to life [1-3]. The photocatalytic activity of TiO_2 relies on the formation of photo-induced charge carries consisting of holes and electrons when UV light is absorbed. Only energy equal to or greater than the band gap of TiO_2, electrons are excited from the valence band (VB) to the conduction band (CB) giving rise to holes at the VB ($TiO_2 + h\nu \rightarrow h_{VB}^{+} + e_{CB}^{-}$) [2]. Upon separation of photo-generated electron–hole pairs, electrons and holes move to the surface of TiO_2. Photo-generated electrons are captured by molecular oxygen adsorbed on the TiO_2 surface, and then superoxide radical anions ($^{\bullet}O_2^{-}$) are generated and undertake reactions with H_2O to yield O^{-} or combine with H^{+} to form hydrogen peroxide (H_2O_2). Positive holes can oxidize OH^{-} or

H_2O at the surface to produce hydroxide radicals ($^{\bullet}OH$), which are extremely powerful oxidants, consequently oxidize organic species into mineral salts, CO_2 and H_2O. Despite their attractive features, such as, high reactivity, chemical stability and non-toxicity, TiO_2 based photocatalysts show three main drawbacks that hinder its cost-effectiveness and applicability [4-6]. They can be listed and explained as follows:

- Wide band gap: TiO_2 nanoparticles depicts a band gap of 3.2 eV which limits their activation at UV light only. Considering that UV light comprises a small part of the solar spectrum (3-5%); the photocatalytic degradation using TiO_2 might be hindered and, in some cases, unfeasible [7].
- Low quantum efficiency: the photocatalytic activity of TiO_2 is usually inhibited by the fast recombination of the photo-generated electron-hole pairs after excitation. This has been associated to low quantum efficiency in TiO_2 systems.
- Agglomeration: the strong tendency of TiO_2 nanoparticles to aggregate may result in a difficult recovering from the solution after treatment and low adsorption capacity for pollutant molecules [8].

Many promising methods have been applied to address the characteristic TiO_2 drawbacks. They can be divided in three main groups: (1) immobilization, (2) Non-metal doping and (3) metal decoration of TiO_2. The immobilization of TiO_2 nanoparticles into porous carriers, such as, silica [9] and carbon [10] structures has been proven to prevent their agglomeration which, in turn, increase the surface area and facilitate recovery processes of the composite photocatalyst after organic compounds mineralization. Here, a natural porous non-metallic mineral, diatomite, was used as carrier because of its ability to effectively immobilize TiO_2 nanoparticles (NPs) [8, 11]. When compared with other TiO_2 structures, the TiO_2/diatomite hybrid photocatalyst shows advantageous ordered pore-size distribution with specific properties such as high amorphous silica content. The huge amount of silicon hydroxyl groups, acid sites and hydrogen bonds on the surface of amorphous SiO_2 can be considered as adsorption sites for pollutants [12, 13]. This enhanced configuration promotes high dye adsorption capacity, improved dispersion, and good recycling ability.

The second approach consists of narrowing the band gap of TiO_2 by creating new energy levels when a non-metal (eg. N and P) replaces O^{2-} or Ti^{4+} in the TiO_2 lattice [14]. By the third method, metal decoration, two mechanisms can be involved to enhance the photocatalytic activity of TiO_2: (I) replacement of Ti^{4+} in TiO_2 lattice by metals which results in a narrow band gap or (II) the use of noble metals to facilitate the electron transfer from TiO_2 to noble metals [15]. In comparison to the studies involving noble metals, transition metal ions and non-metal doped TiO_2 photocatalysts, there is a limited amount of reports about the use of rare-earth metals as dopants, such as, Cerium [16, 17]. The improved photocatalytic activity of (rare-earth metals)-TiO_2 has been related to a decrease of the electron-hole recombination rate through electron capture by the incompletely occupied 4*f* and empty 5*d* orbitals of rare-earth metals. Furthermore, doping with rare earth element has been reported as a promising alternative to enhance TiO_2 thermal stability and to preserve textural properties [18].

The vast literature on TiO_2-hybrid photocatalysts suggests a deep study of specific systems and combinations. In this paper, we systematically investigate how metal-doping and nano-confinement synergistically contribute to reduce the band gap, enhance the quantum efficiency and recovery of the TiO_2 NPs after treatment. We devoted particular attention to understand the effect of Ce- on the structural, textural and morphological properties of TiO_2/diatomite hybrid catalysts obtained from simple sol-gel method. Moreover, the photocatalytic activity of Ce- or La-doped hybrids for the degradation of Rhodamine B (RhB) in aqueous solution at ambient conditions was investigated.

2. Experimental

2.1 Materials

Titanate ($C_{16}H_{36}O_4Ti$, TBOT), ethanol (C_2H_5OH), hydrochloric acid (HCl), acetic acid (CH_3COOH), and Rhodamine B (RhB) were purchased from Beijing Reagent Co. (Beijing, China), which were all

analytical reagent grade without any further purification before using. The Cerium(III) nitrate hexahydrate and Lanthanum(III) nitrate hexahydrate (Aldrich) salt was used as-received without any purification.

2.2 Preparation of Ce-TiO_2/diatomite hybrid catalysts

Immobilization of Ce-TiO_2 into purified natrual diatomite surface was performed as follows[19]. At first, diatomite (1.0 g) with Ce at molar ratios ranging from 0.5 to 3.0% were dispersed in a mixture composed by 14.0 mL of ethanol and 1.0 mL of acetic acid, under stirring for 30 min. Afterwards 1.5 mL of TBOT were added dropwise into the diatomite suspension, under continuous stirring, followed by the addition of 12.0 mL of ethanol:water solution (v:v=1:1; pH=2) which led the hydrolysis of the TBOT at moderate rate. The mixture was then stirred continuously for 12 h to immobilize the as-generated TiO_2 colloids on the diatomite surface. The final product was dried in an oven at 105^{o}C for 4 h and subsequently, calcinated (750 ^{o}C for 2 h in air, heating rate of 2.5°/min).

2.3 Characterization

UV-visible light absorption experiments were carried out in a Varian Cary 500 UV-Vis spectrophotometer equipped with diffusive reflectance accessory ranging from 200 to 800 nm. The crystal phase properties of the samples were analysed with a D8 Advanced X-ray diffractometer (Bruker, Germany) equipped with Cu Kα radiation (λ=0.154056 nm) in the 2θ range from 10 to 80º with a scan rate of 4º/min. The average crystallite size was calculated based on Scherrer's equation ($d = 0.9\lambda / \beta cos\theta$), where λ denotes the wavelength of X-rays and β is the corrected full width at half maxima (FWHM). Raman spectra of the samples were taken on the Renishaw inVia Raman spectrometer with a 514 nm Argon laser line. Both the spectral resolution and the accuracy in the Raman shift are estimated to be ~2 cm^{-1}. The morphology of hybrid catalysts was observed with Tecnai F20 equipped with an energy dispersive X-ray (EDX) analysis. The photoluminescence (PL) spectra of the samples were measured with Horiba Fluorolog-3 spectrometer using the 320 nm line of Xe lamp as the excitation source. XPS spectra were recorded using an X-ray photoelectron spectrometer (XPS-PHI 5600-ci spectrometer, Physical Electronics) without charge compensation. Survey and high resolution spectra were acquired at a detection angle of 45°, using the Kα line of a standard (non-monochromatized) Al (hv=1486.6 eV) and Mg (hv=1253.6 eV) X-ray sources respectively, operated at 300 W. The curve fitting for the high resolution C1s core level peaks was done using Casa XPS software by means of least square peak fitting procedure using a Gaussian–Lorentzian function. The quality of peak detection was evaluated by the maximal residual standard deviation (residual STD) method.

2.4 Photocatalytic experiments

2.4.1 Kinetic test

Rhodamine B (RhB) was used as model pollutant to evaluate the photocatalytic activity of the as-prepared Ce- and La-TiO_2/diatomite hybrid catalysts through a kinetic test. Aliquots were withdrawn from 100 mL of standard RhB aqueous solution (10 mg/L) containing 0.05 g of catalyst (un-doped, Ce-doped or La doped TiO_2/diatomite). Firstly, the suspensions were stirred in the dark for 1 hour to evaluate the adsorption performance. After establishing the equilibrium of adsorption, the photocatalytic reactions were carried out under simulated sunlight irradiation afforded by a 500 W Xe lamp. All the collected samples of RhB solution were analyzed by UV-vis spectrophotometer (UV-9000S, Shanghai Yuanxi). The absorbance was measured at 562 nm. The percentage of RhB degradation (D_R) was calculated by **Eq. 1**:

$$D_R = \frac{C_0 - C_t}{C_0} \times 100\% \quad (1)$$

where C_0 and C_t are the concentrations of RhB before and after degradation, respectively.

2.4.2 Reusability test

Reusability tests were conducted, as described elsewhere [20], for the best Ce-doping concentration tested, based on the photocatalytic activity results acquired from previous section (**2.4.1**). Briefly, the

selected photocatalyst (after being used in degradation test of RhB) was allowed to settle down naturally in the reactor tube (~ 30 min). After, it was rinsed three times with a mixture composed of ethanol and distilled water (ratio 1:1, v:v). The washed material was then dried at 105 °C overnight before being in a new RhB degradation experiment. Four additional tests were conducted and kinetic curves were plotted for each respective cycle.

3. Results and discussion

3.1 XRD Analysis

XRD patterns of Ce-doped TiO_2/diatomite composites are shown in **Fig. 1**. All samples depicted two characteristic diffraction peaks at 2θ = 21.4° and 27.2° corresponding to quartz (coming from diatomite). The crystal plane (101) of anatase was observed at 2θ = 25.3º. The presence of dissolved dopants altered the peak heights and areas, thereby altering the relative intensities of the XRD peaks (lattice distortion). The characteristic peak of the crystal plane (110) of rutile was observed at 27.5º only for the un-doped TiO_2/diatomite. This demonstrates that the Ce-doping inhibited the transition of anatase to rutile phase (referred as ART) at the temperature-time conditions applied. It has been suggested that the effect of dopants cations on the ART is closely related to their valences and ionic radii. Small cations of low valence (<4) should accelerate the ART due to the increase in oxygen vacancies that result from the assumed substitution of Ti^{4+} ions with cations of lower valence. In an opposite way, large cations of high valence (>4) are supposed to replace Ti ions on the anatase lattice, this gives rise to the elimination of existing oxygen vacancies and the formation of Ti interstitials of the same or lower valence [21].

The crystal size of the samples was calculated by using Scherrer's formula (mentioned above in **Section 2.3**) and listed in **Table 1**. As observed, by increasing the concentration of Ce, the crystal size of the Ce-doped TiO_2/diatomite was gradually decreased. This can be explained by the fact that lanthanide oxides may lead to Ti—O—Ce interaction with TiO_2 which blocks of the Ti—O species at the interface with TiO_2 domains stabilizing them, hiding the agglomeration of TiO_2 and thus preventing their growth [6, 22]. That mechanism can prevent ART and promote stabilization of the anatase phase [7, 23], as no rutile peak was observed in the XRD patterns of the Ce-doped TiO_2/diatomite (**Figs. 1b-e**). The preservation of anatase phase after metal doping was confirmed by Raman analysis. As observed by **Fig.2**, the significant vibration peaks of Raman spectra are centred at around 144, 196, 396, 516, and 638 cm^{-1} which are, respectively, the characteristic E_g, E_g, B_{1g}, $A_{1g}+B_{1g}$, and E_g modes depicted by TiO_2 anatase phase [24, 25].

3.2 UV-visible Diffuse Reflectance Spectra (UV-vis DRS) Analysis

Fig. 3a depicts the diffusive reflectance spectra and optical band gap determination of the Ce-TiO_2/diatomite composites. It is well-known that pure TiO_2 shows absorption only in the UV-light region (λ≤387 nm) [26], which is associated to the excitation of electrons from O 2*p* to Ti 3*d* electronic orbital [16]. **Fig.3a** shows that, in comparison to the spectrum of un-doped TiO_2/diatomite composites, Ce-doped TiO_2/diatomite presented better absorption intensity in UV-light region and an absorption tail in the region from 400 to 700 nm. This absorption shift to the visible-light region can be related to the formation of isolated impurities in the energy levels below the bottom of conduction band (CB). For example, in the Ce-doped samples, the appearance of Ce 4*f* electronic state in the middle of the TiO_2 band gap together with the distance of charge transfer between *f* electrons of Ce ions can narrow the band gap of TiO_2 leading to visible-absorption as a response [5, 27].

The bandgap energy was estimated from **Eq. 2**, by extrapolating to zero a linear fit to a plot of $(F(R)h\nu)^{1/2}$ against $h\nu$:

$$F(R)h\nu = A(h\nu - E_g)^2 \quad (2)$$

where $F(R)$ stands for the Kubelka-Munk function (**Eq. 3**) calculated from the reflectance spectrum; and $h\nu$ is the photon energy expressed in eV.

$$F(R) = \frac{(1-R)^2}{2R} \quad (3)$$

The band gap values are summarized in **Table 1**. In the molar ratio range tested (from 0.5 to 3.0%), the band gap decreased as the molar ratios of Ce-TiO_2 increased to a certain value. For the combination properties of the band structures of TiO_2 and CeO_{2-y}, it can be assumed the formed Ti—O—Ce bonding which is mainly composed by Ti 3*d* and localized unoccupied Ce 4*f*, while the valence band is mainly composed by O 2*p* [28]. It means that when the light energy is higher than E_{Ce4f}-E_{vb}, the electrons in valence band can transmit to Ce 4*f* level. Another reason of the visible-light response is due to the presence of Ce_2O_3 in the sample, which can be activated by the presence of a $4f^1 \leftrightarrow 5d^1$ electronic transition under UV and visible light [29]. The lowest band gap value (2.75 eV) was reached at the Ce/Ti molar ratio equals to 1.5%, indicating there was an appropriate doping concentration. Comparing to Ce-doped hybrids, all the La-doped samples we tested display a blue shift in the UV-vis DRS (**Fig. 3b**), which suggested a declined visible-light activity. This indicates that the electron configuration of dopant metal is crucial to the photocatalytic activity of the doped catalyst.

3.3 XPS Analysis

The XPS spectra of un-doped and Ce-doped TiO_2/diatomite composites displayed the obvious Ti, O and Si element peaks, as expected. In **Fig. 4a**, Ti2p peaks of TD were found at 458.9 eV representing $Ti2p_{3/2}$ and 464.6 eV representing $Ti2p_{1/2}$ with a spin-orbital doublet splitting of 5.7 eV, which indicates that the Ti elements mainly existed as Ti^{4+} [30, 31]. Comparing to un-doped TiO_2/diatomite composite, the binding energy of Ti2p of Ce-doped samples varied slightly because of the difference of electronegativity between Ti and dopants [32, 33]. This variation also confirmed that there was corresponding Ti—O—Ce interaction with TiO_2 nanoparticles, as aforemetioned.

The deconvolution of the O1s spectrum of 1.5%-Ce-doped TiO_2/diatomite showed four peaks (**Fig. 4b**), including a dominant peak at about 533.4 eV and three lower energy peaks at approximately 532.4, 530.6 and 529.9 eV. The fitting peaks are assigned to Si− O bonding (SiO_2 of diatomite), surface hydroxyl and adsorbed oxygen mainly from adsorbed water molecules, and Ti− O bonding [34], which account for 39.66%, 16.10%, 5.59% and 38.64% relative atomic percentage of O in 1.5%-Ce-doped TiO_2/diatomite, respectively. The shift observed in Ti—O binding energy might be ascribed to the formation of Ti—O—Ce interaction, due to the lower electronegativity of Ce (1.1) than that of Ti (1.5). The peak area around 530.6 eV for 1.5%-Ce-doped TiO_2/diatomite is larger than that of undoped sample, indicating the higher amount of adsorbed oxygen on 1.5%-Ce-doped TiO_2/diatomite surface. Thus, the trapped electrons in Ce^{4+}/Ce^{3+} pair can be transferred to the oxygen present in the system and also influence the degradation of the dye molecules. Furthermore, the ceria-based oxides can release the oxygen when the oxygen concentration in the system is low due to their good ability to store oxygen [7].

The XPS of 1.5%-Ce-doped TiO_2/diatomite for Ce3d are shown in **Fig. 4c**. The spectrum for Ce3d is rather complex because of the hybridization of Ce3d and Ti2p orbitals and splitting of peaks. According to the previous reports [32, 35, 36], the Ce3d spectrum can be assigned $3d_{3/2}$ spin-orbit states and $3d_{5/2}$ states, around 902.6 eV and 885.1 eV respectively. This indicates the presence of Ce^{3+} in a greater percentage than the Ce^{4+} in the sample, which was helpful in the shifting of the absorption toward the visible region as observed in **Fig. 3a**, and also beneficial for the photo-generated electron capture, consequently giving rise to the enhancement of the photocatalytic performance of the catalyst.

3.4 TEM Analysis

Bright field TEM image of pure diatomite, un-doped, Ce-doped and La-doped TiO_2/diatomite composites are shown by **Figs. 5a to 5e**, respectively. The inset is EDS of un-doped TiO_2/diatomite composite (**Fig. 5b**) and demonstrates the presence of Si, Ti and O; meanwhile Cu signal is derived from the cooper grid for TEM measurement. High-resolution transmission electron microscopy (HRTEM) was

performed to the un-doped TiO_2/diatomite composite (**Fig. 5c**). From **Fig. 5a**, it can be observed that the diatom exhibits highly porous disk-like shape with radius of ca. 30–40 μm. The clean and even surface of the diatom with regular pores of 50–100 nm may represent a benefit to adsorb pollutant molecules when it is used as the photocatalyst support [12]. TEM images, illustrated by **Figs. 5b** to **6e**, revealed that the TiO_2 particles exhibit irregular spherical shapes with low level of agglomeration. The particle size is distributed in a range of 20–40 and 15–25 nm for the un-doped and Ce-TiO_2/diatomite composites, respectively. This data is in general agreement with the XRD determination. The particle observed in **Fig. 5e** (La-TiO_2/diatomite composites) further shrinked than that of Ce-doped sample, which may relate to the blue shift in UV-vis DRS measurement. The nanoparticles showed lattice spacing of d = 0.354 nm for the (101) plane of the anatase phase (**Fig. 5c**) [37]. Besides that, it is noteworthy that TiO_2 particles were still tightly anchored on the surface of diatom during the preparation of the TEM specimen even after a long time of sonication. It demonstrates there was a strong interfacial anchoring strength between the TiO_2 nanoparticles and the diatom matrix, which could decrease the drain of photocatalytic components during the practical applications.

3.5 Photoluminescence Spectra Analysis

Photoluminescence (PL) spectra are useful to understand the behaviour of photo-generated electrons and holes in photocatalysts since PL emission is observed upon occurrence of recombination of electrons and holes. The PL spectra of un-doped, Ce-doped and La-doped TiO_2/diatomite samples in the wavelength range of 350-500 nm with excitation at 320 nm are shown in **Fig. 6**. In comparison to un-doped TiO_2/diatomite, PL intensity of the 1.5%-Ce-TiO_2/diatomite composite decreases largest. The decreased recombination of electrons and holes in Ce-TiO_2 diatomite is favour to enhance the photocatalytic activity. In case of Ce-TiO_2/diatomite composites: The downward trend observed for the diatomite composites is un-doped TiO_2 >Ce-TiO_2(0.5%) >Ce-TiO_2(1.0%) >Ce-TiO_2(3.0%) >Ce-TiO_2(1.5%), which is consistent with the results of UV-vis DRS. This quenching in the intensity of PL spectra is because of Ce^{4+} ions, acting as a Lewis acid, are apparently superior to the oxygen molecule (O_2) in the capability of trapping electrons [29, 38]. All the photo-generated electrons then react with O_2 adsorbed on the TiO_2 surface and generate $\bullet O_2^-$ radicals. Accordingly, it can be hypothesized that photocatalytic activity of these Ce-doped samples may be enhanced. The peak intensity centred at 468 nm decreases first and then increases when the quantity of the Ce was surpassed 1.5%. This indicates that the excess doping may create the recombination centers for the produced electrons and holes because the thickness of the space-charge layer decreases with an increase of dopant content [7]. Consequently, the photocatalytic activity decreased as discussed later.

3.6 Photocatalytic Activity of Ce-TiO_2/diatomite Hybrid

The photocatalytic activity of the prepared catalysts was evaluated by performing degradation experiments of 10 mg/L aqueous solution of Rhodamine B (RhB) with simulated sunlight illumination. Kinetic plots of the Ce-doped samples with different molar ratios of Ce are shown in **Fig. 7a**. They were fitted by the apparent first-order rate equation (**Eq. 4**) as follows:

$$-Ln\left(\frac{C}{C_0}\right) = kt \tag{4}$$

where C is the RhB concentration at time t, and k is the apparent reaction rate constant.

Table 2 lists the percentage of RhB degradation (D_R) values and k of un-doped and Ce-doped TiO_2/diatomite composites. The increase of D_R and k upon metal-doping can be related to the fact that the Ti 3*d* and localized unoccupied Ce 4*f* composes of Ti—O—Ce bonding and the redox Ce^{4+}/Ce^{3+} pair present on the surface of TiO_2 acts as an electron scavenger. The trapped electrons in Ce^{4+}/Ce^{3+} pair can be transferred to the oxygen present in the system and subsequently degraded the substrate dye molecules. Therefore, the presence of the Ce^{4+}/Ce^{3+} pair can efficiently separate the electrons and holes. However, when the molar ratio of Ce was greater than 1.5% the dopants created the recombination centres for the photo-generated electrons and holes, undermining the photocatalytic activity. The highest removal ratio and

kinetics value were reached at the Ce/Ti molar ratio equals to 1.5%, where also reached the lowest intensity of PL emission. To the contrary, La-doped samples which have a blue shift in UV-vis DRS (**Fig. 3b**) and the higher PL emission intensity (**Fig. 6**), subsequently show the lower photo-degradation rate for RhB. Another contributing factor for the enhanced activity is assumed due to the unfully oxidized surface, indicating the existence of some oxygen vacancies and Ce_2O_3 which has the capability of a $4f^1 \leftrightarrow 5d^1$electronic transition under UV and visible light.

The quality of our results can be proved by comparing them with existing reports on the photo-degradation percentage obtained for Ce-doped TiO_2 catalysts. At our best composition tested, 1.5%-Ce-doped, RhB removal was similar to that reported by Xie et al. [32] and Liu et al. [39] during the photo-degradation of RhB by Ce-TiO_2 based catalysts. However, the content of photoactive material (Ce-TiO_2) in our synthesized catalysts is, excluding diatomite, approximately 0.013 g which is substantially lower than that reported elsewhere (usually 0.1 g of Ce-TiO_2) [32, 39]. This indicates that the proposed hybrid catalyst (Ce-TiO_2/diatomite) shows advantages in a cost-effective way for industrial application.

3.7 Reusability of Ce-TiO_2/diatomite composite

The recovery and reusability are key features for the application of photocatalysts in water remediation. Reusability test was conducted for the best experimental condition, Ce-doped TiO_2/diatomite (1.5%), based on the results of photocatalytic activity described by **Table 2**. **Fig. 8** shows that the Ce-doped TiO_2/diatomite (1.5%) catalyst could be efficiently reused even after four reaction cycles. Although the formed intermediates were not characterized in this work, there is a vast literature exploring different reaction of intermediates from Rhodamine B [40-42]. As an example, in recent publication, Cui et al. demonstrated that benzoic acid was the major identifiable breakdown intermediate during the photo-degradation of Rhodamine B over Ag modified ferroelectric $BaTiO_3$ under simulated solar light [43].

4. Conclusions

The photocatalytic activity of Ce-TiO_2/diatomite composites for dye RhB was systematically investigated and compared with un-doped and La-doped TiO_2/diatomite composite. The best Ce/Ti molar ratio was found at 1.5%, where the bandgap energy was decreased from 3.17 (un-doped TiO_2/diatomite composite) to 2.75 eV; and the percentage of RhB degradation (D_R) reached 72.03% under simulated sunlight irradiation. By UV-vis DRS, XPS and PL, it was possible to conclude that the redox Ce^{4+}/Ce^{3+} pair played an important role on the surface of TiO_2 acting as an electron scavenger. The localized unoccupied Ce 4*f* level has also contributed for the improved photocatalytic properties. This study demonstrates that the use of diatomite as support for the Ce-doped TiO_2 nanoparticles is a potential strategy to enable the application of TiO_2 in a real wastewater remediation treatment.

Acknowledgments

The authors gratefully acknowledge the financial support provided by National Technology R&D Program in the 12th five years plan of China (2011BAB03B07), the National Nature Science Foundation of China (grant NO. 21274006, 51503005), Beijing science and technology leading talent project (LJ201614), Beijing BaiQianWan Talents Program, the Importation and Development of High-Caliber Talents Project of Beijing Municipal Institutions -the Beijing Great Wall Scholars Incubator Program (CIT&TCD20150306), the Beijing City Board of Education Upgrade Project (NO. TJSHG201310012021), the Project of Construction of Innovative Teams and Selection and Development of Excellent Talents for Beijing Institute of Fashion Technology (PTTBIFT) and the Open Project Program of Beijing Key Laboratory (NO. 2015ZK-02).

The first author thanks the China Scholarship Council (CSC) for financial support. And also the first author appreciates Professor Ian R. Gentle's suggestion and support, which make the first author be able to do experiments in School of Chemistry and Molecular Biosciences, The University of Queensland.

References

[1] M. Pelaez, N.T. Nolan, S.C. Pillai, M.K. Seery, P. Falaras, A.G. Kontos, P.S. Dunlop, J.W. Hamilton, J.A. Byrne, K. O'Shea, A review on the visible light active titanium dioxide photocatalysts for environmental applications, Appl. Cataly. B: Environmental, 125 (2012) 331-349.
[2] A. Fujishima, X. Zhang, Titanium dioxide photocatalysis: present situation and future approaches, C. R. Chim., 9 (2006) 750-760.
[3] J. Lyu, L. Zhu, C. Burda, Considerations to improve adsorption and photocatalysis of low concentration air pollutants on TiO_2, Cataly. Today, 225 (2014) 24-33.
[4] D.M. Tobaldi, R.C. Pullar, A.S. Škapin, M.P. Seabra, J.A. Labrincha, Visible light activated photocatalytic behaviour of rare earth modified commercial TiO_2, Mater. Res. Bull., 50 (2014) 183-190.
[5] M. Nasir, S. Bagwasi, Y. Jiao, F. Chen, B. Tian, J. Zhang, Characterization and activity of the Ce and N co-doped TiO_2 prepared through hydrothermal method, Chem. Eng. J., 236 (2014) 388-397.
[6] M. Nasir, J. Zhang, F. Chen, B. Tian, Detailed study of Ce and C codoping on the visible light response of titanium dioxide, Res. Chem. Intermediat., 41 (2015) 1607-1624.
[7] M. Nasir, Z. Xi, M. Xing, J. Zhang, F. Chen, B. Tian, S. Bagwasi, Study of synergistic effect of Ce- and S-codoping on the enhancement of visible-light photocatalytic activity of TiO_2, J. Phys. Chem. C, 117 (2013) 9520-9528.
[8] B. Wang, F.C. de Godoi, Z. Sun, Q. Zeng, S. Zheng, R.L. Frost, Synthesis, characterization and activity of an immobilized photocatalyst: Natural porous diatomite supported titania nanoparticles, J. Colloid. Interf. Sci., 438 (2015) 204-211.
[9] A. Pal, T.K. Jana, K. Chatterjee, Silica supported TiO_2 nanostructures for highly efficient photocatalytic application under visible light irradiation, Mater. Res. Bull., 76 (2016) 353-357.
[10] R. Leary, A. Westwood, Carbonaceous nanomaterials for the enhancement of TiO_2 photocatalysis, Carbon, 49 (2011) 741-772.
[11] B. Wang, G. Zhang, Z. Sun, S. Zheng, Synthesis of natural porous minerals supported TiO_2 nanoparticles and their photocatalytic performance towards Rhodamine B degradation, Powder Technol., 262 (2014) 1-8.
[12] Z. Sun, C. Bai, S. Zheng, X. Yang, R.L. Frost, A comparative study of different porous amorphous silica minerals supported TiO_2 catalysts, Appl. Cataly. A: General, 458 (2013) 103-110.
[13] M. Rafatullah, O. Sulaiman, R. Hashim, A. Ahmad, Adsorption of methylene blue on low-cost adsorbents: A review, J. Hazard. Mater., 177 (2010) 70-80.
[14] R. Asahi, T. Morikawa, T. Ohwaki, K. Aoki, Y. Taga, Visible-light photocatalysis in nitrogen-doped titanium oxides, Science, 293 (2001) 269-271.
[15] M. Wang, J. Ioccozia, L. Sun, C. Lin, Z. Lin, Inorganic-modified semiconductor TiO_2 nanotube arrays for photocatalysis, Energ. Environ. Sci., 7 (2014) 2182-2202.
[16] W. Xue, G. Zhang, X. Xu, X. Yang, C. Liu, Y. Xu, Preparation of titania nanotubes doped with cerium and their photocatalytic activity for glyphosate, Chem. Eng. J., 167 (2011) 397-402.
[17] X. Lu, X. Li, J. Qian, N. Miao, C. Yao, Z. Chen, Synthesis and characterization of CeO_2/TiO_2 nanotube arrays and enhanced photocatalytic oxidative desulfurization performance, J. Alloys Compd., 661 (2016) 363-371.
[18] M. Meksi, The role of lanthanum in the enhancement of photocatalytic properties of TiO_2 nanomaterials obtained by calcination of hydrogenotitanate nanotubes, Appl. Catal. B: Environmental, 181 (2016) 651-660.
[19] Z. Sun, X. Yang, G. Zhang, S. Zheng, R.L. Frost, A novel method for purification of low grade diatomite powders in centrifugal fields, Int. J. Miner. Process., 125 (2013) 18-26.
[20] B. Wang, G. Zhang, X. Leng, Z. Sun, S. Zheng, Characterization and improved solar light activity of vanadium doped TiO_2/diatomite hybrid catalysts, J. Hazard. Mater., 285 (2015) 212-220.
[21] D.H. Hanaor, C. Sorrell, Review of the anatase to rutile phase transformation, J. Mater. Sci., 46 (2011) 855-874.
[22] L.Q. Jing, X.J. Sun, B.F. Xin, Wang. Baiqi, W.M Cai., H.G. Fu, The preparation and characterization of La doped TiO_2 nanoparticles and their photocatalytic activity, J. Solid State Chem., 177 (2004) 3375-3382.
[23] Q. Wang, S. Xu, F. Shen, Preparation and characterization of TiO_2 photocatalysts co-doped with iron (III) and lanthanum for the degradation of organic pollutants, Appl. Surf. Sci., 257 (2011) 7671-7677.

[24] Z. Zhang, C. Shao, L. Zhang, X. Li, Y. Liu, Electrospun nanofibers of V-doped TiO_2 with high photocatalytic activity, J. Colloid. Interf. Sci., 351 (2010) 57-62.
[25] S. Sahoo, A.K. Arora, V. Sridharan, Raman line shapes of optical phonons of different symmetries in anatase TiO_2 nanocrystals, J. Phys. Chem. C, 113 (2009) 16927-16933.
[26] D. Mitoraj, H. Kisch, The Nature of Nitrogen-modified titanium dioxide photocatalysts active in visible light, Angew. Chem. Int. Ed., 47 (2008) 9975-9978.
[27] J. Xu, Y. Ao, D. Fu, C. Yuan, Study on photocatalytic performance and degradation kinetics of X-3B with lanthanide-modified titanium dioxide under solar and UV illumination, J. Hazard. Mater., 164 (2009) 762-768.
[28] M. Tian, H. Wang, D. Sun, W. Peng, W. Tao, Visible light driven nanocrystal anatase TiO_2 doped by Ce from sol–gel method and its photoelectrochemical water splitting properties, Int. J. Hydrogen Energ., 39 (2014) 13448-13453.
[29] F.B. Li, X.Z. Li, M.F. Hou, K.W. Cheah, W.C.H. Choy, Enhanced photocatalytic activity of Ce^{3+}-TiO_2 for 2-mercaptobenzothiazole degradation in aqueous suspension for odour control, Appl. Catal. A: General, 285 (2005) 181-189.
[30] T. Yu, X. Tan, L. Zhao, Y. Yin, P. Chen, J. Wei, Characterization, activity and kinetics of a visible light driven photocatalyst: Cerium and nitrogen co-doped TiO_2 nanoparticles, Chem. Eng. J., 157 (2010) 86-92.
[31] B.M. Reddy, P.M. Sreekanth, Y. Yamada, Q. Xu, T. Kobayashi, Surface characterization of sulfate, molybdate, and tungstate promoted TiO_2-ZrO_2 solid acid catalysts by XPS and other techniques, Appl. Catal. A: General, 228 (2002) 269-278.
[32] J. Xie, D. Jiang, M. Chen, D. Li, J. Zhu, X. Lü, C. Yan, Preparation and characterization of monodisperse Ce-doped TiO_2 microspheres with visible light photocatalytic activity, Colloids Surf. Physicochem. Eng. Aspects, 372 (2010) 107-114.
[33] Y.H. Xu, Z.X. Zeng, The preparation, characterization, and photocatalytic activities of Ce-TiO_2/SiO_2, J. Mol. Catal. A: Chem., 279 (2008) 77-81.
[34] B.M. Reddy, P.M. Sreekanth, E.P. Reddy, Y. Yamada, Q. Xu, H. Sakurai, T. Kobayashi, Surface Characterization of La_2O_3−TiO_2 and V_2O_5/La_2O_3−TiO_2 Catalysts, J. Phys. Chem. B, 106 (2002) 5695-5700.
[35] Z. Liu, B. Guo, L. Hong, H. Jiang, Preparation and characterization of cerium oxide doped TiO_2 nanoparticles, J. Phys. Chem. Solids, 66 (2005) 161-167.
[36] B.M. Reddy, A. Khan, Y. Yamada, T. Kobayashi, S. Loridant, J.-C. Volta, Structural characterization of CeO_2−TiO_2 and V_2O_5/CeO_2−TiO_2 catalysts by raman and XPS techniques, J. Phys. Chem. B, 107 (2003) 5162-5167.
[37] X. Yang, L. Xu, X. Yu, Y. Guo, One-step preparation of silver and indium oxide co-doped TiO_2 photocatalyst for the degradation of rhodamine B, Catal. Commun., 9 (2008) 1224-1229.
[38] Y. Xie, C. Yuan, Visible-light responsive cerium ion modified titania sol and nanocrystallites for X-3B dye photodegradation, Appl. Catal. B: Environmental, 46 (2003) 251-259.
[39] Y. Liu, P. Fang, Y. Cheng, Y. Gao, F. Chen, Z. Liu, Y. Dai, Study on enhanced photocatalytic performance of cerium doped TiO_2-based nanosheets, Chem. Eng. J., 219 (2013) 478-485.
[40] K. Yu, S. Yang, H. He, C. Sun, C. Gu, Y. Ju, Visible light-driven photocatalytic degradation of rhodamine B over $NaBiO_3$: Pathways and mechanism, J. Phys. Chem. A, 113 (2009) 10024-10032.
[41] H. Fu, C. Pan, W. Yao, Y. Zhu, Visible-light-induced degradation of rhodamine B by nanosized Bi_2WO_6, J. Phys. Chem. B, 109 (2005) 22432-22439.
[42] F. Chen, J. Zhao, H. Hidaka, Highly selective deethylation of rhodamine B: Adsorption and photooxidation pathways of the dye on the TiO_2/SiO_2 composite photocatalyst, Int. J. Hydrogen Energ., 5 (2003) 209-217.
[43] Y. Cui, S.M. Goldup, S. Dunn, Photodegradation of rhodamine B over Ag modified ferroelectric $BaTiO_3$ under simulated solar light: Pathways and mechanism, RSC Advances, 5 (2015) 30372-30379.

Figure captions:

Figure 1: XRD patterns of (a) un-doped and (b-e) Ce-doped TiO_2/diatomite composites with different concentration from 0.5% to 3.0%.

Figure 2: Raman spectra of (a) un-doped and (b-e) Ce-doped TiO_2/diatomite composites with different concentration from 0.5% to 3.0%.

Figure 3: UV-visible diffuse reflectance spectra and optical band-gap determination of un-doped and Ce-, La-doped TiO_2/diatomite composites.

Figure 4: XPS spectra of 1.5%-Ce/TiO_2 diatomite composite (a) Ti2p, (b) O1s and (c) Ce3d.

Figure 5: Bright field TEM image of (a) pristine diatomite, (b-c) un-doped TiO_2/diatomite composite, (d) 1.0%-Ce-TiO_2/diatomite composites and (e) 1.0%-La-TiO_2/diatomite composites.

Figure 6: Photoluminescence spectra of the samples with the excitation wavelength of 320 nm for un-doped TiO_2/diatomite composites, Ce-TiO_2/diatomite composites at different Ce-TiO_2 molar ratios and 1.5%-La-TiO_2/diatomite composites.

Figure 7 Time courses (a) and first-order kinetics plots (b) of photo-degradation of RhB over Ce-doped TiO_2/diatomite composites with various doping content from 0.5% to 3.0%.

Figure 8: Reusability test of 1.5%-Ce-doped TiO_2/diatomite composite.

Fig.1

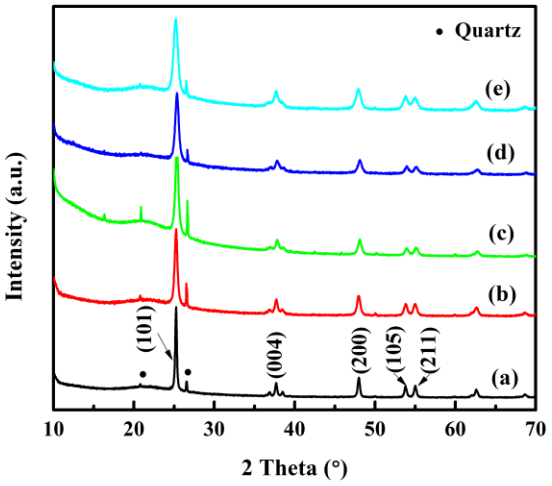

Fig. 1

Fig.2

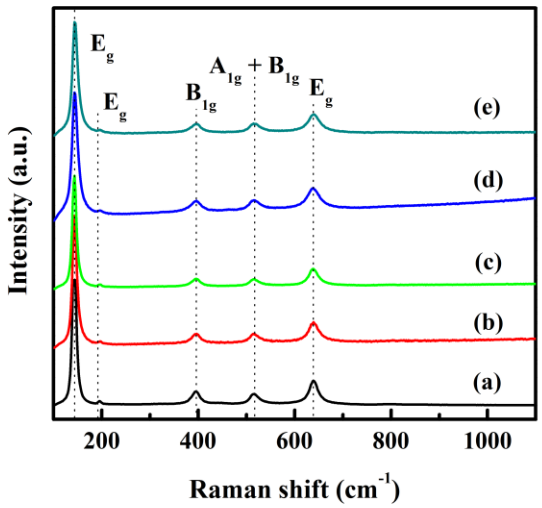

Fig. 2

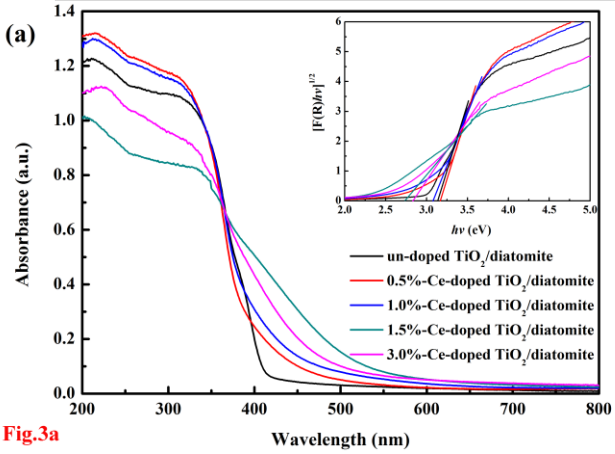

Fig.3a

Fig. 3a

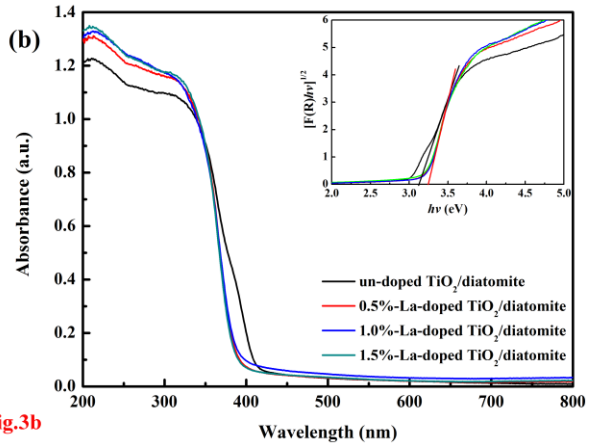

Fig.3b

Fig. 3b

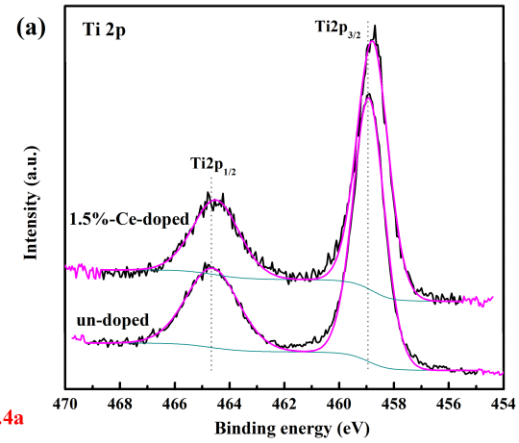

Fig.4a

Fig. 4a

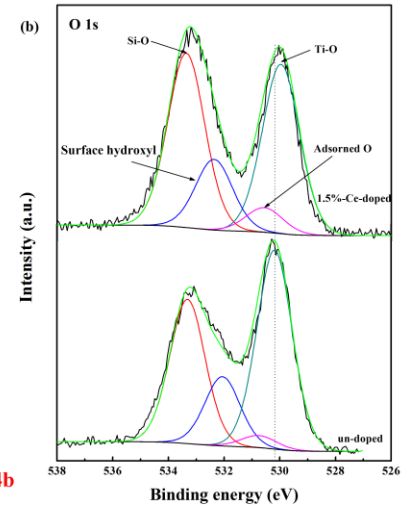

Fig.4b

Fig. 4b

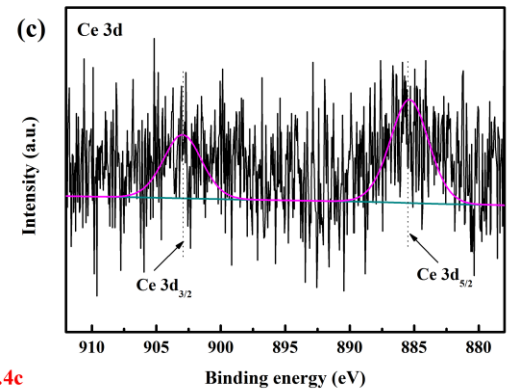

Fig.4c

Fig. 4c

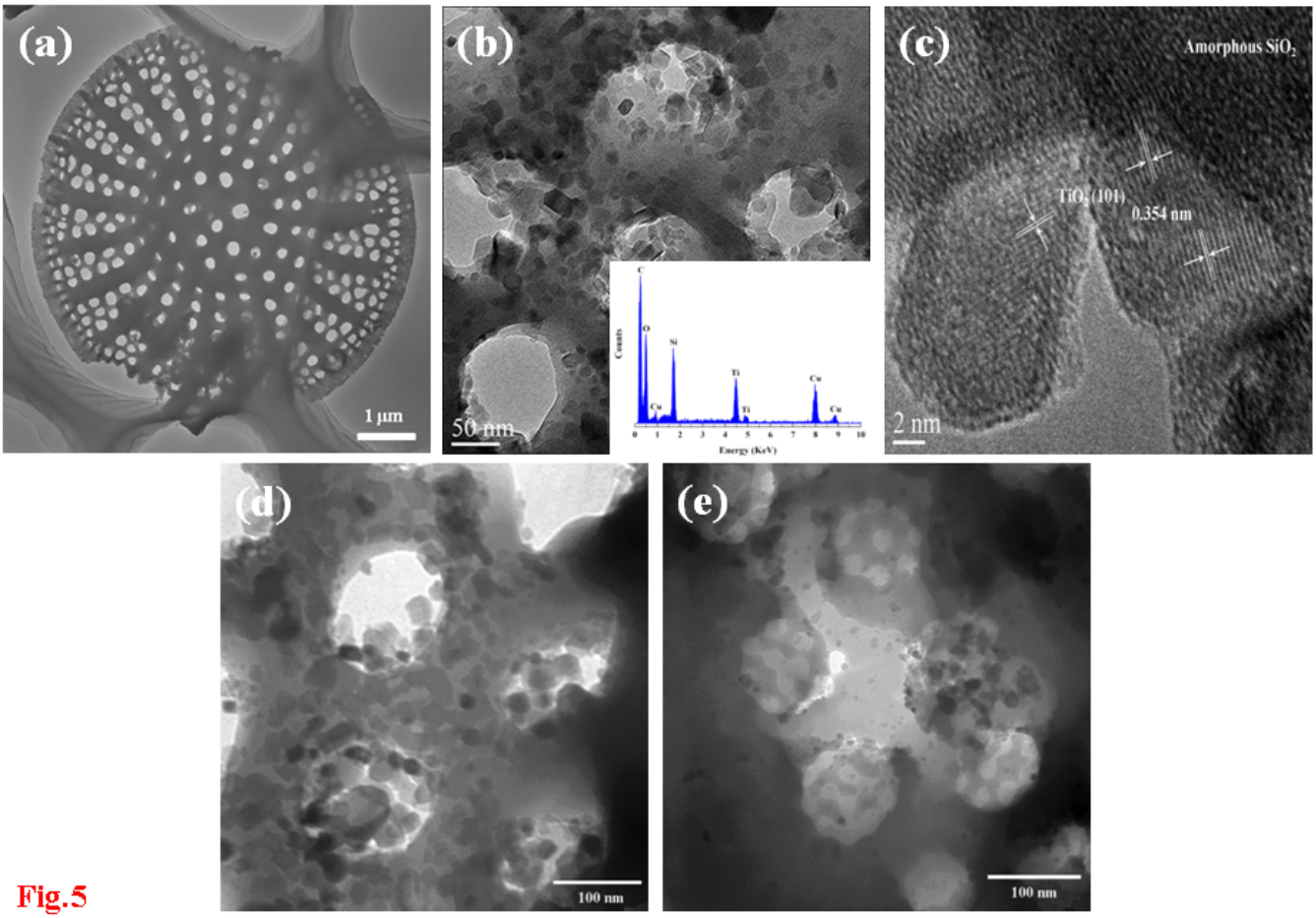

Fig.5

Fig. 5

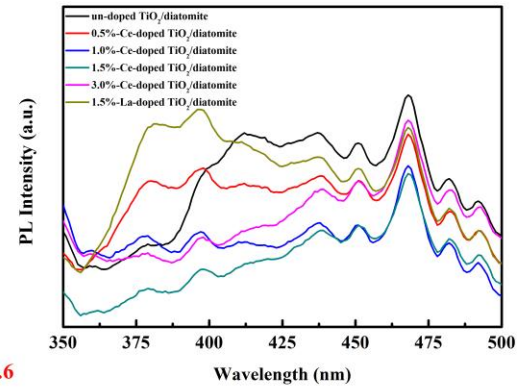

Fig.6

Fig. 6

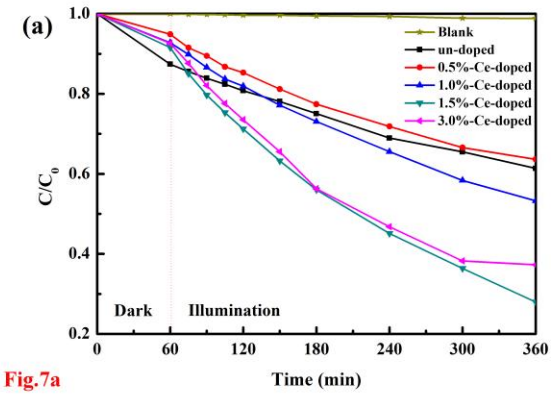

Fig.7a

Fig. 7a

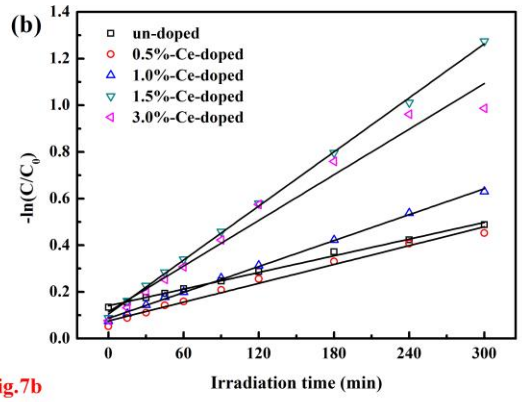

Fig.7b

Fig. 7b

Fig.8

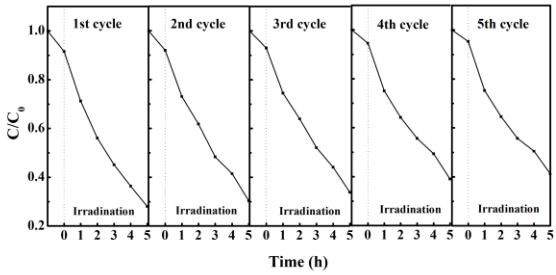

Fig. 8

Graphical Abstract

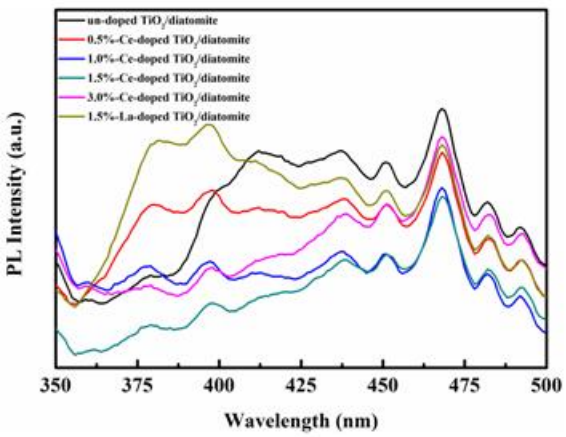

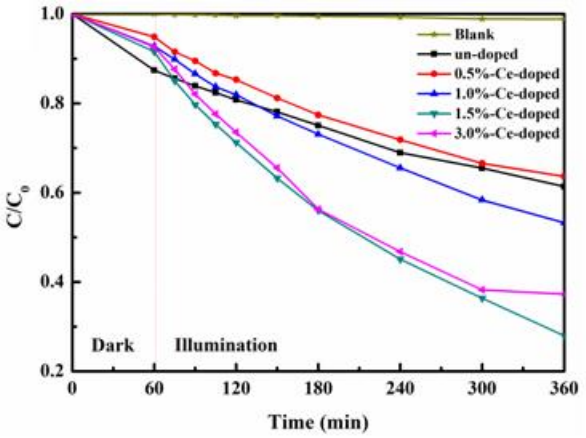

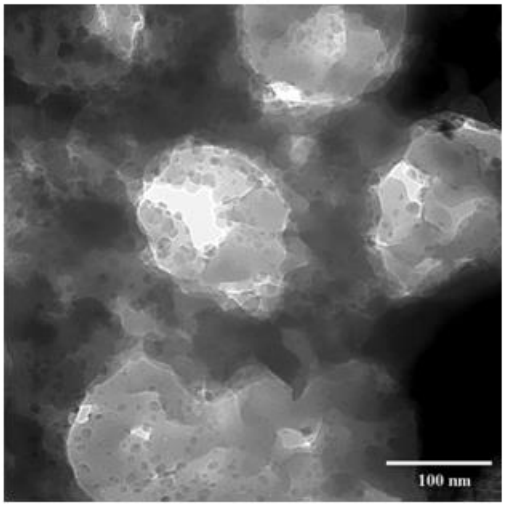

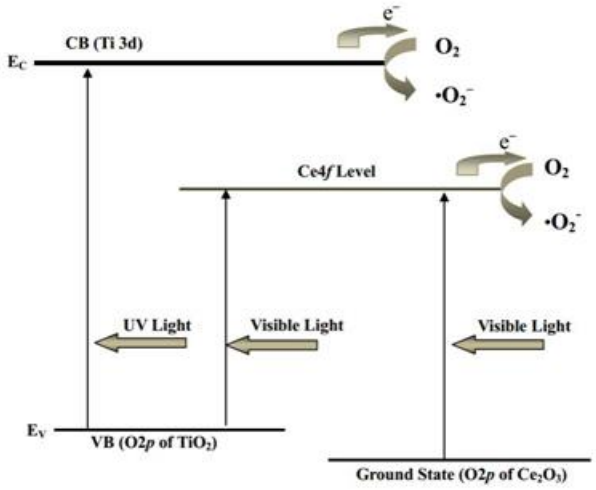

Highlights

- Lanthanide cations doped TiO_2/diatomite composite photocatalyst were synthesized.
- The physiochemical property and sunlight photoactivity were characterized.
- The presence and influence of cerium in TiO_2 matrix were systematically analyzed.
- The reasonable deductions of the visible-light activity of cerium doped samples were given.

Table 1: Bandgap energies and crystal size of TiO_2/diatomite composite with and without Ce-doping.

M	Molar ratio (%)	Size of $A_{(101)}$ (nm)	Size of $R_{(110)}$ (nm)	Bandgap energy (eV)
Ce	0.5	20.10	-	3.14
	1.0	18.62	-	3.06
	1.5	16.29	-	2.75
	3.0	13.66	-	2.83
Un-doped TiO_2/diatomite		31.98	24.10	3.17

Table 2: Photocatalytic activity of un-doped and Ce-, La-doped TiO_2/diatomite composites

M	Molar ratio (%)	Solar light irradiation		
		D_R (%)	k (10^{-3} min^{-1})	R^2
Ce	0.5	36.39	1.34	0.98601
	1.0	46.75	1.85	0.99817
	1.5	72.03	3.86	0.99913
	3.0	61.75	3.26	0.95991
La	0.5	36.41	1.33	0.97714
	1.0	36.87	1.35	0.9895
	1.5	38.22	1.40	0.98871
Un-doped TiO_2/diatomite		38.64	1.19	0.99611